Integrative and Comparative Biology

Integrative and Comparative Biology, volume 58, number 2, pp. 317–328
doi:10.1093/icb/icy044

Society for Integrative and Comparative Biology

SYMPOSIUM

Differentiation and Induced Sensorial Alteration of the Coronal Organ in the Asexual Life of a Tunicate

Lucia Manni,[1] Chiara Anselmi,[2] Paolo Burighel, Margherita Martini and Fabio Gasparini

Dipartimento di Biologia, Università degli Studi di Padova, Via U. Bassi 58/B, 35121 Padova, Italy

From the symposium "Integrative Biology of Sensory Hair Cells" presented at the annual meeting of the Society for Integrative and Comparative Biology, January 3–7, 2018 at San Francisco, California.

[1]E-mail: lucia.manni@unipd.it

[2]E-mail: chiara.anselmi.3@phd.unipd.it

Synopsis Tunicates, the sister group of vertebrates, possess a mechanoreceptor organ, the coronal organ, which is considered the best candidate to address the controversial issue of vertebrate hair cell evolution. The organ, located at the base of the oral siphon, controls the flow of seawater into the organism and can drive the "squirting" reaction, i.e., the rapid body muscle contraction used to eject dangerous particles during filtration. Coronal sensory cells are secondary mechanoreceptors and share morphological, developmental, and molecular traits with vertebrate hair cells. In the colonial tunicate *Botryllus schlosseri*, we described coronal organ differentiation during asexual development. Moreover, we showed that the ototoxic aminoglycoside gentamicin caused morphological and mechanosensorial impairment in coronal cells. Finally, fenofibrate had a strong protective effect on coronal sensory cells due to gentamicin-induced toxicity, as occurs in vertebrate hair cells. Our results reinforce the hypothesis of homology between vertebrate hair cells and tunicate coronal sensory cells.

Introduction

Fifteen years ago, a novel mechanoreceptor organ, the coronal organ, was described in the oral siphon of the colonial tunicate *Botryllus schlosseri* (Burighel et al. 2003). Tunicates are marine, filter-feeding invertebrates that are considered to be the vertebrate sister group (Kocot et al. 2018). In this respect, coronal cells are of interest for researchers studying vertebrate evolution. Like vertebrate hair cells, coronal cells are receptor cells without own axons (referred here as secondary receptors) and thus they can contribute to the investigation of vertebrate hair cell evolution. The coronal organ is located at the base of the oral siphon and is responsible for the "squirting" reaction (Mackie et al. 2006): when cells are stimulated by contact with potentially dangerous particles that enter the siphon with seawater flow, the animal stops the inflowing current and contracts its body muscles to expel these particles. The organ is composed of one or a few more rows of sensory cells flanked by supporting cells, bordering the edge of the oral velum and tentacles (Caicci et al. 2010). Sensory cells are contacted at their base by neurites that come from elsewhere (i.e., from the cerebral ganglion), as occurs in vertebrate hair cells innervated by afferents that derive from the ear (Dabdoub et al. 2016). Vertebrate hair cells are also innervated by efferent fibers (Sienknecht et al. 2014). Moreover, as in vertebrate hair cells, coronal cells possess a hair bundle, delimited by supporting cell apical protrusions, to detect the stimulus.

Hair cells of the ear and the lateral line system are mechanoreceptors that mediate vibrational and fluid-flow sensing that allow hearing, balance, and vibrational sensing (Chagnaud et al. 2017). Loss of hair cells is an important cause of deafness in humans because lost cells are typically not replaced (Burns and Stone 2017). In mammals, this loss occurs because of age and/or use of therapeutics drugs, such as aminoglycoside antibiotics, which can destroy both hair cells and their innervating neurons. Hair cells and associated sensory neurons

Advance Access publication June 26, 2018

develop from cranial placodes, in particular, from otic and lateral line placodes, which are thickened areas of the cranial ectoderm expressing a particular set of developmental genes (Schlosser et al. 2014). Cranial placodes, together with neural crests, are classically considered to be exclusive to vertebrates and crucial for the evolution of their features (Gans and Northcutt 1983; Northcutt and Gans 1983). The discovery hair cell-like coronal cells raises the possible earlier evolution of placodes in tunicates (Manni et al. 2001).

Since the first coronal organ description, many steps have been taken. The coronal organ is now considered to be a tunicate synapomorphy (Caicci et al. 2013; Rigon et al. 2013). The organ has a complex connectivity system, with involvement in afferent, efferent, and reciprocal synapses with neurites (Burighel et al. 2011; Rigon et al. 2018). Moreover, axo-dendritic contacts and synapses between neurites and supporting cells are also recorded (Burighel et al. 2003). Sensory cells have diverse hair bundles in different species: mono-, bi-, or pluri-ciliated bundles with microvilli or stereovilli, the latter of which are sometimes graded in length. Some neurotransmitters are localized in the coronal organ (Rigon et al. 2018), such as glutamate (which mediates afferent hair cell inputs) and acetylcholine, GABA, and serotonin (which are involved in efferent stimulation to hair cells).

Morphological and molecular development of the coronal organ have been analyzed in the tunicate *Ciona sp.* (Gasparini et al. 2013a; Rigon et al. 2018). Sensory cells are first identified during larval metamorphosis, before tentacles form, as cells with short cilia and microvilli. Sensory cells undergo gradual differentiation, acquiring their definitive morphology in juveniles. Different from those in vertebrates, in *Ciona*, not only supporting cells, but also sensory cells can proliferate and accompany tentacle growth during the lifespan (Gasparini et al. 2013a). Some of the genes involved in hair cell differentiation (*Atoh*, *Notch*, *Delta-like*, *Hairy-b*, and *Musashi*) (Fritzsch and Elliott 2017) are expressed in the developing coronal organ (Rigon et al. 2018). Moreover, the embryonic territory that is the origin of the oral siphon and therefore the tentacles and velum is a thickened ectodermal epithelium (called "anterior proto-placode") expressing homologs of some placodal genes (Patthey et al. 2014). In *B. schlosseri*, placodal genes are also expressed in the territory that gives rise to the oral siphon in buds produced by asexual reproduction (Gasparini et al. 2013b).

Tunicates develop from an embryo in which the chordate body plan is recognizable. However, in colonial species, such as *B. schlosseri*, sexual reproduction is accompanied by asexual reproduction (blastogenesis), permitting colony growth (Manni et al. 2007; Gasparini et al. 2015). In *B. schlosseri*, three blastogenic generations coexist and synchronously develop in the colony: the adult, filter-feeding blastozooids, their buds, and budlets on buds. Cyclically, adult blastozooids regress and are substituted in filtration by their buds, which open their siphons (Cima et al. 2010). This cyclical event, called a change of generation (or takeover), is accompanied by the transformation of budlets in buds and the formation of a new generation of budlets in the latter. Adult filtering individuals formed through the two developmental pathways are morphologically similar and can be used as correspondent experimental models (Manni and Burighel 2006; Brunetti et al. 2017). This feature extends comparisons between blastozooid and vertebrate structures, as in the case of the blastozooid and vertebrate pharynx, which are considered to be homologous. In this species, coronal sensory cells possess an immobile cilium surrounded or flanked by a corolla of short stereovilli (Burighel et al. 2003). A fibrillary fuzzy coat extends radially to establish connections between adjacent stereovilli and between the stereovilli and ciliary shaft. At the base of coronal sensory cells, the plasmalemma forms a groove in which neurites are located.

From an evo-devo perspective, understanding coronal organ development and function could provide insights into the evolution of vertebrate hearing and balance, which will likely facilitate the development of new therapies for hair cell loss in humans. Here, we explore both the development of the coronal organ during blastogenesis and the effect of an ototoxic agent, the aminoglycoside gentamicin, on coronal organ morphology and functional mechanoreceptivity in *B. schlosseri*.

Materials and methods

Animals and whole-mount preparation

Specimens of *B. schlosseri* (family Styelidae, order Stolidobranchia) were collected from the lagoon of Venice and reared and staged according to Sabbadin's (1955) technique (reviewed in Manni et al. [2014] and Cima et al. [2015]). Blastozooids are grouped in star-shaped systems around the common cloacal siphon.

Colonies were anesthetized with MS 222, fixed in Bouin's fluid, washed in 50% ethyl alcohol, rehydrated, and stained with Mayer's hematoxylin. After washing in distilled water, colonies were

Table 1 Number of tested colonies and zooids, and implemented treatments

	Gentamicin				Fenofibrate	Fenofibrate + Gentamicin
No. of colonies	4	8	2	6	5	7
No. of zooids	169	334	86	255	204	286
Treatment	0.65 mg/mL ×24 h	1.3 mg/mL ×24 h	2.6 mg/mL ×1 h	2 mg/mL ×2 h	50 µM ×45 min	[50 µM×45 min]+ [2 mg/mL×2 h]

dehydrated in alcohol and mounted with balsam. For the acetylcholinesterase (AChE) reaction, colonies were treated according to Zaniolo et al. (2002). To control reaction specificity, the substrate was omitted, or the specific inhibitor 0.03 M neostigmine bromide (Cat. No. N2001, Sigma–Aldrich) was added. Buds were studied with light microscopy.

Electron microscopy

Colonies were anesthetized, fixed, postfixed, dehydrated, and embedded as described in Franchi et al. (2016). For transmission electron microscopy (TEM), thick sections (1 µm) were counterstained with toluidine blue and thin sections (60 nm) were contrasted with uranyl acetate and lead citrate. Micrographs were taken with a FEI Tecnai G12 electron microscope operating at 75 kV.

For scanning EM (SEM), pieces of colony containing adult blastozooids were anesthetized and fixed as described for TEM, but not postfixed. After dehydration with ethanol, the pieces were dissected to expose the oral velum and tentacles. Specimens were air-dried after hexamethyldisilazane (Sigma–Aldrich, H4875) washes at increasing concentrations (30% and 70% in EtOH, and then two washes of 100%, 15 min each). Specimens were sputter-coated with gold-palladium and observed under a FEI Quanta 200 SEM.

Gentamicin and/or fenofibrate treatment and behavioral response

Colonies immediately after the takeover were treated with gentamicin (LFM, 80 mg/2 mL) and/or fenofibrate (Sigma–Aldrich, F6020). Colonies were immerged in a petri dish filled with one or both drugs in seawater as indicated in Table 1.

For SEM, eight colonies were treated with gentamicin solution (2 mg/mL ×2 h), and six control colonies were processed.

Before and after treatment with gentamicin and/or fenofibrate, the reaction of about 40 (34–45) zooids *per* colony to the tentacle stimulation test (TST) was tested. The colonies used were 32 in total. The test consisted of a single mechanical stimulation of the tentacle rim, gently touching it with a glass needle prepared with a Narishige PD-5 horizontal capillary puller mounted on a Singer Mk1 micromanipulator. The response repeatability to TST was verified during the phase of method development taking into consideration the following variables: operators, instruments, lot of reagents, elapsed time between TST implemented pre- and post-drug treatment, rearing temperature, and stage of blastogenesis. During protocol development zooids responded consistently to repeated stimulation. Commonly the expected reaction of zooids to the TST is a typical squirting behavior consisting of sudden atrial siphon closure and vigorous body contraction (Mackie et al. 2006). In our experiments, three primary different categories of reaction were observed: (i) squirting behavior, (ii) faint and anomalous reaction (i.e., absence of atrial siphon closure and/or faint-to-absent body contraction), and (iii) not perceptible reaction; for simplicity, we call these reactions "fast," "faint," and "null," respectively. The TSTs were performed under a Leica MZ6 stereomicroscope.

Statistical analyses

Data on behavioral response were grouped in samples of percentages as follow (see Supplementary Material 01):

> Type i: zooids *per* colony with absence of squirting reaction before treatment, and zooids *per* colony with absence of squirting reaction after treatment.
> Type ii: zooids *per* colony changing behavior after the treatment.

Statistical analyses were performed using R Software Environment, version 3.4.3 (R Core Team 2017). Samples were visualized in box-and-whisker plots. For each dataset, the following statistical pipeline was used. The Shapiro test was used to determine whether each sample was normally distributed. Bartlett test or in case of normality violation, Fligner–Killeen test was used to verify the homogeneity of variances among samples in each dataset. For each implemented treatment (Table 1), a dataset of paired samples (before and after treatment) was tested for the equality of the means with the non-parametric Wilcoxon signed-rank test. The

non-parametric one-way ANOVA equivalent, Kruskal–Wallis rank sum test, was used to verify the null hypothesis of equality of medians among samples; subsequently, in case of rejection of the null hypothesis, the Conover's test with Bonferroni *p*-value adjustment and quantiles corrected for ties (Pohlert 2014) were used to calculate the pairwise multiple comparisons between samples.

Summarizing, the following two testing methods were applied:

Testing method 1. Comparison of the means for two samples of paired data (before and after each single treatment, "type i" samples);
Testing method 2. ANOVA and *post hoc* test, using two different groups of samples:
Group (a) A sample formed from data collected before treatments, and other samples each formed from data collected after a treatment ("type i" samples);
Group (b) Samples formed from data of zooids *per* colony changing behavior after treatment ("type ii" samples).

For both testing methods, the statistical test pipeline was conducted twice, i.e., using two datasets (dataset 1: samples obtained from only null reactions; dataset 2: samples from both null and faint reactions). In regard to the zooids that changed their behavior after treatments (Testing method 2, Group b), two datasets were obtained considering zooids with a decreased intensity of reaction after treatment (dataset 1: from fast to null reaction; dataset 2: from fast to faint reaction, plus from faint to null reaction, plus from fast to null reaction) (see Supplementary Material 01). Statistics were considered significant when the values were <0.05.

Results

Development of tentacles and velum and coronal organ organization

The coronal organ in *B. schlosseri* is located at the base of the oral siphon, on the ring of tentacles, and velum (Fig. 1A–E). The thin epithelial fold that connects the tentacles is the velum. Both the tentacles and velum form during bud development from a thickened epithelium at the base of the oral siphon rudiment (Fig. 1F–K). During their differentiation, the oral siphon is closed. The two lateral tentacles are first recognizable in the early bud as small projections departing from the velum (Fig. 1F,G), successively; in mid-cycle, the ventral and the dorsal tentacles also became visible (Fig. 1H,I). These four

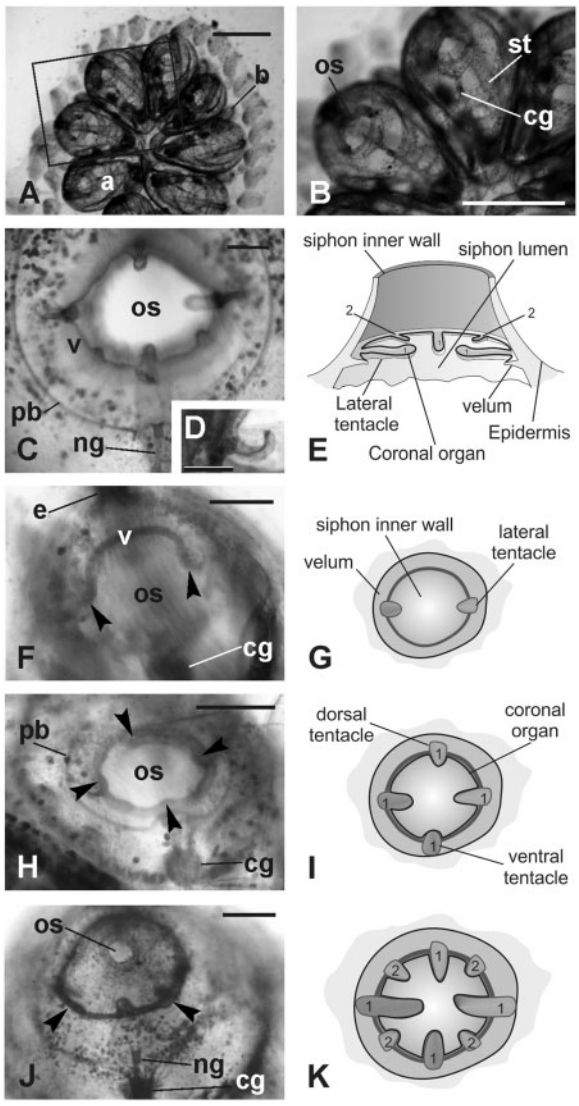

Fig. 1 Oral siphon development. Whole mounted colonies. (**A**–**B**) Dorsal views of a colony in mid-cycle. The square area in A is enlarged in B to show the adult blastozooid organization. (**C**–**D**) Oral siphon in an adult blastozooid in mid-cycle. The four first order tentacles and two of the second order tentacles are recognizable (the other two are out of focus). A thin velum (v) joins the tentacles. Note in D that the upper surface of the tentacle is spoon shaped. (**E**) Schematic drawing of the oral siphon in adult blastozooid. 1, first order tentacles; 2, second order tentacles; (**F**–**K**) Tentacles and velum development in buds; oral siphons closed. F, H, and J: whole mount specimens, dorsal view. G, I, and K: sketches of oral siphon rudiment (ventral view) corresponding to the stages shown in F, H, and I, respectively (i.e., early, mid, and late cycle buds, respectively). In F, lateral tentacles (arrowheads) and velum (v) are recognizable. In H, the four first order tentacles are visible (arrowheads). In J, two of the second order tentacles (arrowheads; 2 in K) are alternated with longer ones that belong to the first order (1). a, adult blastozooid; b, bud; cg, cerebral ganglion; ng, duct of the neural gland; os, oral siphon; pb, peripharyngeal band; st, stigma. Scale bars: A and B, 1 mm, C, D, F, H, and J, 100 μm.

tentacles represent the first order tentacles; later, four smaller tentacles, belonging to the second order, form alternate to those of the first order (Fig. 1J,K). When the zooid is completely developed, the siphon opens and filtration begins: the tentacles reach their typical length and the coronal organ is fully differentiated (Fig. 2A–D).

Coronal organ differentiation

During early bud development, the oral siphon rudiment consists of two epithelial components: the outer component one is the epidermis; the inner component (called oral siphon inner epithelium) is a disk of tunic secreting cells facing the branchial chamber (Fig. 2E,F). The tunic represents a useful marker to distinguish the oral siphon inner epithelium from the adjacent cells of the forming branchial chamber. The oral siphon outer and the inner components approaches during bud development and eventually fuses together, permitting the siphon aperture. During siphon development, the two components are separated by the hemocoel in which hemocytes move and muscle cell precursors differentiate (Fig. 2E–H). These precursors will form the sphincter muscle of the siphon (Degasperi et al. 2009). Posteriorly, the siphon rudiment is close to the neural complex rudiment. This is composed of the rudiments of a neural gland, which is opened into the branchial chamber by means of a duct, the dorsal organ, and the cerebral ganglion.

The coronal sensory epithelium is derived from a ring of thickened epithelium that forms around the oral siphon inner epithelium. At the stage at which the heart begins beating (Fig. 2G–I), this epithelium (including the presumptive sensory area) forms from cylindrical cells resting on a basal lamina. Cells have a large nucleus with nucleolus and are rich in free ribosomes, whereas mitochondria and RER cisterns are rare. A thick glycocalyx covers the cell apical surface; the basal profile is smooth. Cells actively proliferate (Fig. 2I). At this stage, the first neurites close to the oral siphon rudiment are recognizable. With the localization of AchE, their path can be followed in detail (Fig. 2J). Nerves reach the oral siphon rudiment from a couple of primary nerves (anterior roots) emerging from the anterior cerebral ganglion. These two nerves, which divide repeatedly, are directed to the anterior tissues. Thin neurites at the base of the lateral tentacle rudiments (Fig. 2J), which form at this stage, are also visible. TEM showed that small neurite sections are in the area of the forming coronal organ (Fig. 2I, inset).

At the mid-cycle stage, numerous neurites are close to the presumptive sensory area (Fig. 2K). The AchE reaction reveals the large pericoronal nerves encircling the siphon and located at the base of the peripharyngeal bands. Nerves split repeatedly into progressively smaller bundles, which eventually reach the numerous muscle fibers of the forming oral sphincter muscle and the differentiating coronal cells. The latter begin to emerge from the epithelium of the velum and tentacles (Fig. 2L,M) and are cylindrical, similar to the adjacent velum/tentacle cells, but they become recognizable for apical and basal features. Apically, sensory cells differentiate a cilium and some short stereovilli, both of which are surrounded by a fibrillary fuzzy coat, whereas the thick glycocalyx was no longer recognizable (Fig. 2L). Basally, the plasmalemma forms a slight groove into which neurites extend (Fig. 2L,M). Synaptogenesis occurs concurrently with coronal cell differentiation. The first synaptic contacts are both conventional contacts between neurites and sensory cells and contacts between adjacent neurites. Supporting cells are recognizable as C-shaped cells flanking and anchoring sensory cells. Apically, supporting cells exhibit a thick glycocalyx (inset in Fig. 2L) and partially cover the sensory cell apex, leaving only the area bearing the sensory hair bundle exposed to seawater. Basally, supporting cells limit the sensory cell groove in which the neurites are located.

In late bud, the velum is clearly recognizable as an epithelial fold at the base of the siphon, well separated by the close peripharyngeal band (Fig. 3A,B). The tunic covering the oral siphon inner epithelium extends to the velum. At this stage, the second order tentacles are formed, and tentacles begin to acquire a spoon shape. The coronal organ reaches the conventional adult configuration (Fig. 3C). Coronal sensory cells are cylindrical, with a round, large nucleus. Their cytoplasm has the features of differentiated cells: the Golgi apparatus is apical, with a field rich in vesicles; mitochondria are numerous; RER cisterns are close to the nuclear membrane; and some lipid droplets are recognizable (Fig. 3D,E). The apical tuft is composed of numerous stereovilli filled with microfilaments, accompanying the cilium. The innervation pattern increases in complexity. Sensory cell basal grooves are deeper than those in previous stages and contain more neurites (Fig. 3F,G). The latter typically have microtubules, occasional mitochondria, and electron-dense vesicles (most likely neurotransmitter vesicles).

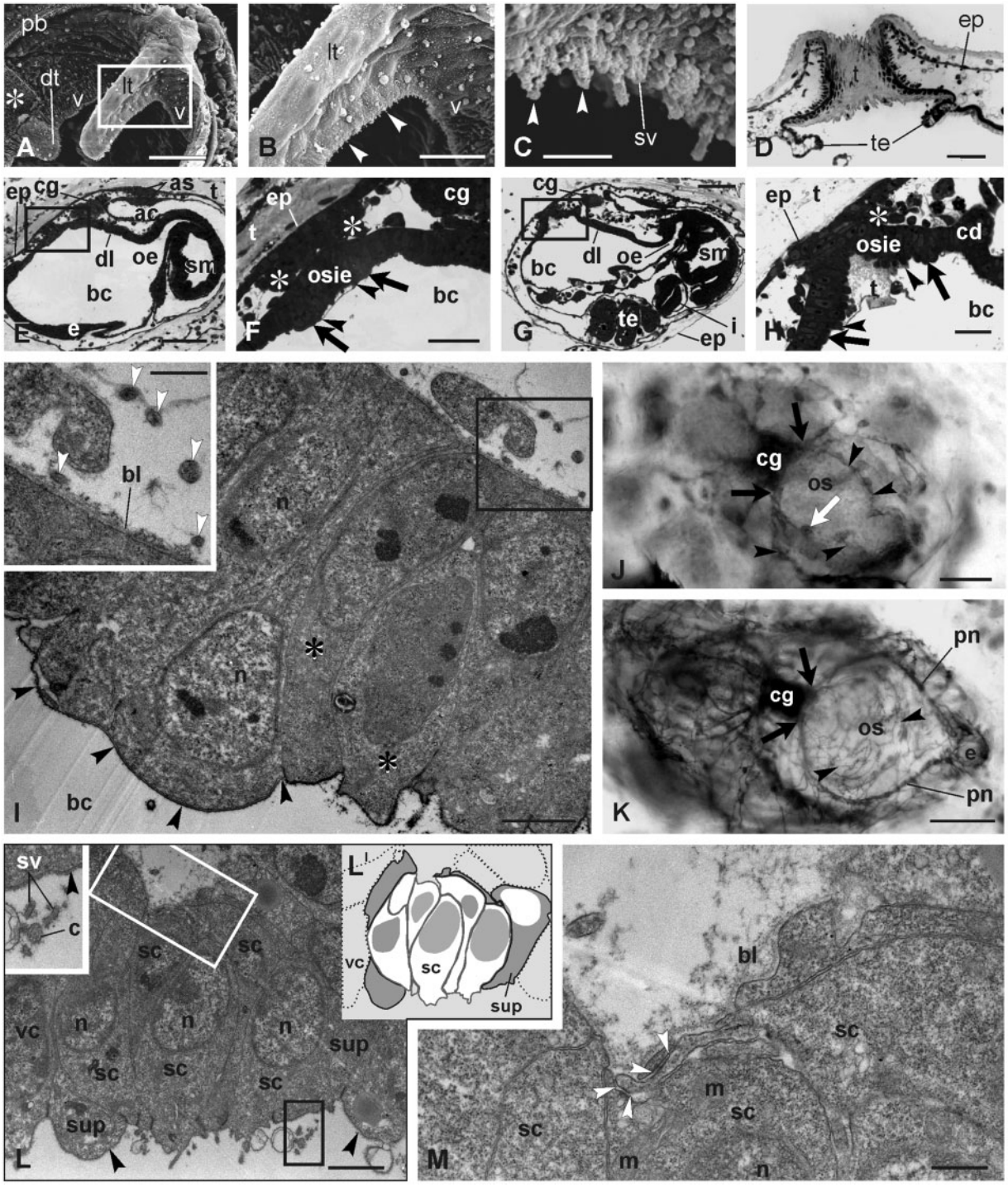

Fig. 2 Coronal organ in adult blastozooids and differentiation in early buds. (**A**–**D**) Adult. (**A**–**C**) SEM of part of the oral siphon viewed from the branchial chamber to show the coronal organ. The square area in A is enlarged in B. Arrowheads point to cilia of coronal sensory cells. Asterisk: ciliated area close to the dorsal tentacle (dt). (D) Transverse section of an oral siphon; the tunic (t) lies on its inner side, partly covering the velum and tentacle (te) upper side. The section is tangential to the siphon wall so that the tunic appears to fill the siphon lumen. Toluidine blue. (**E**–**H**) Sagittal medial sections of two early cycle buds at the beginning of the cycle (earlier stage in E–F). The square areas in E and G are enlarged in F and H, respectively, to show the details of the oral siphon rudiment. The oral siphon inner epithelium (osie, borders marked by arrowheads) and epidermis are covered by the tunic; asterisks: muscle cell precursors. Arrows: velum area. Toluidine blue. (**I**) Mitotic cells (asterisks) within the velum/tentacles epithelium. Black arrowheads: thin tunic layer covering the apex of the oral siphon inner epithelium. The squared area is enlarged in the inset. White arrowheads: neurites close to the velum/tentacles area. TEM. (**J**–**K**) AChE reaction on a bud in early- (J) and mid-cycle (K) in dorsal view. Arrowheads: neurites reaching the oral siphon rudiment. The cerebral ganglion and nerves are marked. White arrow in J: forming right

Morphological and sensorial effects of gentamicin and/or fenofibrate treatments on the coronal organ

SEM was used to investigate the morphology of the coronal organ of adult zooids in colonies treated with gentamicin compared with that of control colonies. Control colonies showed the typical coronal arrangement of a continuous ciliary row (see Fig. 2A–C), whereas in treated colonies, the continuity of this row was altered with scattered interruptions (Fig. 4A).

The three primary types of zooid reaction (fast, faint, and null) were usually observed both in control and treated colonies.

Because some null and faint reactions could be due to some possible errors in touching and/or

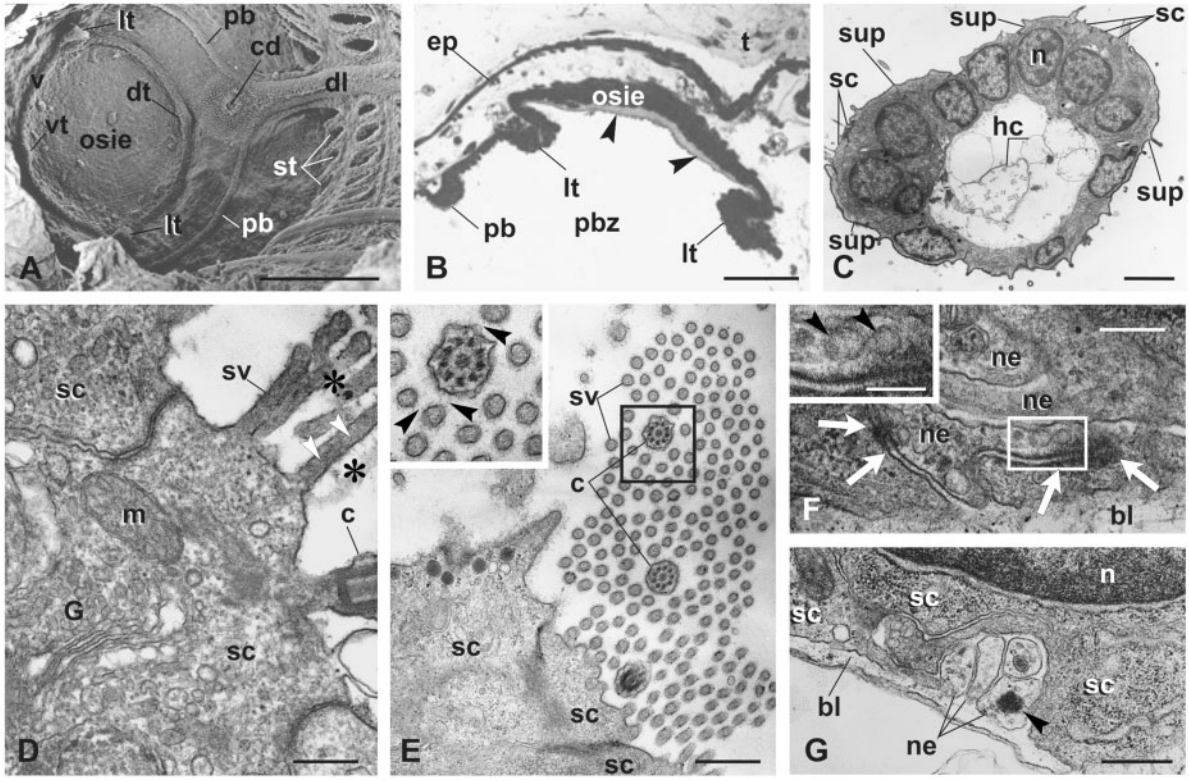

Fig. 3 Coronal organ differentiation in mid bud. (**A**) SEM of the oral siphon rudiment viewed from the branchial chamber. The siphon is closed. The peripharyngeal band (pb) marks the border between the anterior prebranchial zone and posterior branchial zone of the pharynx. Developing velum (v) and first order tentacles are visible (lt, the two lateral ones; dt, the dorsal one; vt, the ventral one). Stigmata (st) are perforated. (**B**) Transverse section of the oral siphon rudiment showing the relationships between the two lateral tentacles (lt), the peripharyngeal band (pb), and the oral siphon rudiment. Arrowheads: tunic produced by the oral siphon inner epithelium (osie). Toluidine blue. (**C**) Transverse section of a tentacle belonging to a bud at a more advanced stage than that shown in A–B. Note the slightly spoon-shaped upper surface facing the inflowing seawater (upper, left). hc, hemocytes in the blood sinus. TEM. (**D**–**E**) Details of the sensory bundle, cut longitudinally in D, transversely in E. Stereovilli and cilium are linked to one another by the fibrillary fuzzy coat (asterisks in D, black arrowheads in inset of E). White arrowheads in D: microfilaments in stereovilli. TEM. G, Golgi field. (**F–G**) Details of sensory cell basal grooves containing neurites (ne) separated from the hemocoel by the basal lamina (bl). Some synaptic contacts are recognizable (white arrows in F). Some vescicles (arrowheads) are within neurites (enlarged in inset in F). TEM. Other symbols as in Fig. 2. Scale bars: A, 100 µm; B, 50 µm; C, 3 µm; D and F, 300 nm; inset in F: 150; and E and G, 600 nm.

lateral tentacle marked by the AChE reaction. Black arrows: anterior nerve roots; pn, pericoronal nerves. Anterior at right-bottom. Whole mount bud. (**L–M**) Detail of differentiating coronal cells in a mid-cycle bud. Oblique cut of the organ in L shows a few sensory cells (schematized in L^{I}; white cells: sensory cells; gray cells: supporting cells; dotted cells: velar cells). Black square, inset in L: stereovilli (sv) and a cilium (c) of a hair bundle, both of which are covered by the fibrillary fuzzy coat. Black arrowheads: thick glycocalyx covers supporting (sup) and velar (vc) cells. Sensory cells lack the covering. In M, the basal groove is enlarged with neurites (white square in L). White arrowheads: first recognizable synaptic contacts. ac, atrial chamber; as, atrial siphon; bc, branchial chamber; bl, basal lamina; cd, ciliated duct of the neural gland; cg, cerebral ganglion; dl, dorsal lamina; e, endostyle; ep, epidermis; i, intestine; lt, lateral tentacle; m, mitochondrion; n, nucleus; oe, esophagus; os, oral siphon; pb, peripharyngeal band; sc, sensory cell; sm, stomach; te, testis lobule; v, velum. Scale bars: A, D, and E, 50 µm; B, F, and G, 20 µm; C, I, and L, 2 µm; H, 5 µm; I (inset), 1 µm; J and K, 100 µm; M, 500 nm.

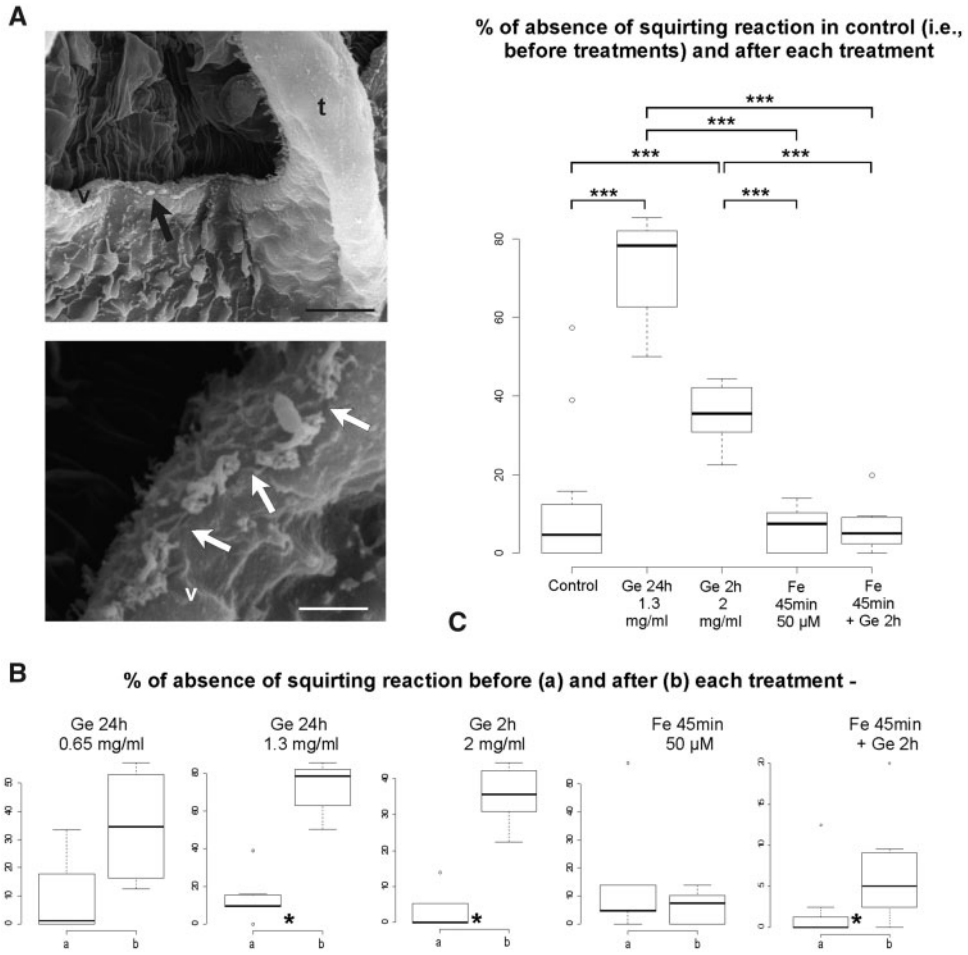

Fig. 4 Gentamicin-induced morphological and mechanosensorial impairments on coronal organ. (**A**) Colonies treated with gentamicin. SEM of part of two oral siphons viewed from the branchial chamber to show the coronal organ on the velum (v) and tentacles (t). Arrows point to some discontinuity of coronal apical tufts. (**B**–**C**) Boxplots of datasets for the following: (B) comparison of means for two samples of paired data (before and after each single treatment) and (C) ANOVA and *post hoc* test among treated samples (samples obtained from data after each treatment) and control (a sample obtained from all data before treatment). Boxplots from the datasets obtained from null plus faint reactions are shown. Ge, gentamicin; Fe, fenofibrate. Asterisks denote significance in the comparisons between samples as follow: * <0.05, ** <0.01, *** <0.001. Scale bars in A: 10 µm (upper) and 2 µm (lower).

individual variation in sensitivity, the statistical test pipeline was conducted twice. The significance of the test was always confirmed in the two pipelines, except in a case of the two-sample comparisons (i.e., fenofibrate followed by gentamicin treatment). The results of the statistical analyses are described below and are shown in Fig. 4B,C only for datasets with null plus faint reactions. Further details on the analyses can be found in Supplementary Materials 02 and 03.

The comparison before and after treatment with gentamicin for 24 h at 0.65 mg/mL indicated no significant effect on the behavioral response to the TST. By contrast, a double concentration of gentamicin (1.3 mg/mL) for the same period significantly increased the absence of the squirting reaction (Fig. 4B). To exclude that a 24 h treatment could overwhelm the protective effect of the fenofibrate pre-treatment, we tested reduced periods of gentamicin treatment. No effect was recorded in zooids from two colonies treated for 1 h at 2.6 mg/mL (data not shown), whereas a significantly altered behavior was observed after treatment for 2 h at 2 mg/mL (Fig. 4B).

The treatment with 50 µM fenofibrate for 45 min, followed by gentamicin at 2 mg/mL for 2 h, resulted in no significant effect on the TST, considering only null reaction data (Supplementary Material 03), but a slight significance was recorded ($0.04 < P\text{-value} < 0.05$) when null and faint reactions were grouped together (Fig. 4B). Finally, treatment with only fenofibrate did not affect zooid behavior.

ANOVAs and *post hoc* tests showed that the results of treatments with fenofibrate and fenofibrate

followed by gentamicin were not significantly different, and these two treatments were not different from the control. Additionally, the tests indicated that both gentamicin treatments strongly affected the reaction to the TST compared with that of the other treatments and the control (Fig. 4C). Finally, the gentamicin treatment at 1.3 mg/mL for 24 h increased the absence of a fast reaction to the TST compared with that of the 2 mg/mL for 2 h treatment, but with significance only when the samples were compared with data from zooids that changed behavior after treatments (see Supplementary Material 03).

Discussion

Coronal sensory cells of tunicates are considered to be putatively homologous to vertebrate hair cells based on recognized relationships at developmental, molecular, and morphological levels (Burighel et al. 2008, 2011; Gasparini et al. 2013a, 2013b; Rigon et al. 2018). In this study, new information on coronal organ cytodifferentiation during asexual reproduction, which is associated with evidence on the morphological and mechanosensorial impairment caused by gentamicin, reinforces this hypothesis.

Coronal organ and innervation pattern development in blastozooids

In this study, we followed the coronal morphogenetic events during *B. schlosseri* asexual development. Differentiation of the organ was studied in sexual development in another species, *Ciona robusta*, previously called *Ciona intestinalis* type A (Brunetti et al. 2015; Pennati et al. 2015), in which differentiation occurs during metamorphosis and in early juveniles (Gasparini et al. 2013a). Different from those of *B. schlosseri* buds, in *Ciona* early juvenile, coronal cells are morphologically recognizable before tentacle and velum development because of the precocious apical bundle appearance. Moreover, the bundle undergoes a deep rearrangement during differentiation, whereas in *B. schlosseri*, the bundle shows the definitive configuration as soon as it is recognizable.

In *Ciona* juveniles, mitoses are detected in both sensory and supporting cells (Gasparini et al. 2013a). This finding suggests that the proliferative ability was found in the ancestors of both cell types but is now restricted to supporting cells in vertebrates and limited in mammals to very small populations of multipotent stem/progenitor cells (Burns and Stone 2017; Xu et al. 2017). Moreover, in *Ciona*, mitoses are hypothesized to sustain coronal organ elongation following the increase of the size and number of tentacles. This elongation is related to animal growth throughout its lifespan, which lasts several months.

In contrast to *Ciona*, *B. schlosseri* adult zooids have a shorter lifespan of few days and do not increase in size, either in tentacle number or length. Mitosis in *B. schlosseri* was recognized in early buds in the presumptive coronal organ territory but not in differentiated coronal cells. Additionally, in the congeneric *Botryllus primigenus* in which the proliferative activity was studied, mitoses were not specifically reported for the adult coronal organ (Kawamura et al. 2008). We hypothesized that the coronal proliferative ability decreases or ceases in botryllid differentiated coronal cells as an adaptation to their short cycle, which involves continuous regression and the formation of new individuals.

In *B. schlosseri*, neurites from the cerebral ganglion reached the presumptive coronal organ territory before coronal sensory cells were morphologically distinguishable. Although we could not exclude that neurites were involved in differentiating oral siphon muscle fibers, neurites within tentacle rudiments and their closeness to presumptive coronal cells strongly support a mutual relationship between coronal cells and associated brain sensory neurons during development. The precocious arrivals of neurites at differentiating organs has been observed in tunicates, also for coronal cells (Zaniolo et al. 2002; Gasparini et al. 2013a): nerves spread among organs well before their cytodifferentiation and before the ganglion reaches its definitive configuration in terms of neuron number and nerves emanating from it. This nerve propagation apparently parallels development in mammal embryos (Elliott et al. 2017) in which segregation of afferent projections appears to develop before peripheral (hair cells) and central (cochlear nucleus neurons) target cell differentiation, although we do not know where the coronal sensory neurons are positioned in the cerebral ganglion nor when they become active. In this respect, both a precise neuronal map of the adult tunicate cerebral ganglion and a cell lineage analysis of sensory neurons would be very useful to refine the homology relationships between coronal sensory cells and vertebrate hair cells by including their sensory neurons.

Gentamicin impairs coronal sensory cells but fenofibrate prevents it

Gentamicin, like other aminoglycoside, is ototoxic, causing hair cell damage by first inducing disarray and disruption of the apical bundle followed by apoptosis (Huth et al. 2011). Research related to ototoxic effects of aminoglycosides primarily focuses on

mammal vestibular hair cells, but the disruptive effect of these drugs on hair cells has also been demonstrated for fish lateral line mechanoreceptors (neuromasts) (Coffin et al. 2009; Fan et al. 2016) and electroreceptors (ampullary organs) (Fan et al. 2016).

Despite some differences, the vertebrate vestibular and lateral line systems are considered to be two evolutionarily related sensory systems that share developmental, morphological, physiological, and molecular traits (Chagnaud et al. 2017). For this reason, the lateral line is currently used as a model to study both the normality of hair cells and pathophysiology of hearing defects because the position on the body surface simplifies experimental treatments *in vivo* (Whitfield 2002) and because the lateral line also grows after embryogenesis (Brignull et al. 2009). Similarly, the coronal organ is accessible and continuously formed throughout the lifespan. However, different from vertebrate hair cells, coronal sensory cells also form by non-self-renewal division (Gasparini et al. 2013a) and during non-embryonic development (present work). In this respect, the coronal organ represents a suitable model for the study of the recovery of damaged secondary sensory cells. Moreover, statistical approaches take advantage of the experimental value of resorting colonial organisms for an appropriate analysis of out-coming data (Gasparini et al. 2014). Indeed, more than in isogenic strains, in *B. schlosseri*, each individual zooid in a colony is essentially a biological replicate that is not perturbed by intrinsic variables, as a clonal individual. Differences among individuals derive only from external perturbations (e.g., experimental variations). Therefore, the statistically powerful results are strongly facilitated.

In this study, SEM analyses demonstrated for the first time the disruptive effect of gentamicin on this mechanoreceptor, showing a loss of coronal sensory cell continuity along the organ. Moreover, the TST on colonies after gentamicin correlated with the morphological analysis, demonstrating a significant decrease of the percentage of zooid with squirting response to the TST with respect to the same colonies before treatment. The treatment duration and concentration influenced animal responses. Therefore, these experiments suggested that the coronal organ not only has the same mechanosensorial function as that of the lateral line/vestibular systems of vertebrates but has also a similar sensibility to gentamicin.

Fenofibrate is a peroxisome proliferator-activated receptor (PPAR) agonist. PPARs protect from reactive oxygen species by increasing antioxidant enzymes in different tissues and organs (Yousefipour et al. 2010; Aleshin and Reiser 2013; Ding et al. 2014). Fenofibrate was first recognized to protect kidneys from oxidative stress by increasing antioxidant enzymes, including catalase and superoxide dismutase-1 (Hou et al. 2010). Recently, fenofibrate has been found to protect hair cells from gentamicin-induced toxicity, both in vestibular and lateral line systems of zebrafish (Park et al. 2017). In this study, we demonstrated that a loss in zooid squirting response did not occur when *B. schlosseri* colonies were preventively treated with fenofibrate, indicating a strong protective effect to coronal sensory cells, as occurs in vertebrate hair cells.

In conclusion, this investigation on coronal organ differentiation, function, and induced damage during the asexual life cycle not only reinforces the hypothesized multi-level homology between secondary sensory cells in Vertebrata and its sister group Tunicata (Kocot et al. 2018) but also has an evo-devo relevance. The study allows us to gain insight into the depicted scenario of the co-option of both morphodynamic mechanisms and genetic pathways during the evolution of coloniality, which characterizes tunicates among chordates (Tiozzo et al. 2006; Gasparini et al. 2008, 2011, 2013b; Ricci et al. 2016).

Acknowledgments

The authors thank Mr. Filippo Ferraro for help in performing behavioral experiments.

Funding

This work was supported by grant from the University of Padova—Progetti di Ricerca di Ateneo [Grant 2015—CPDA153837] and by the National Institute on Deafness and Other Communication Disorders of the National Institutes for Health [Grant number: R13-DC017092] by L.M.

Supplementary data

Supplementary data available at *ICB* online.

References

Aleshin S, Reiser G. 2013. Role of the peroxisome proliferator-activated receptors (PPAR)-α, β/δ and γ triad in regulation of reactive oxygen species signaling in brain. Biol Chem 394:1553–70.

Brignull HR, Raible DW, Stone JS. 2009. Feathers and fins: non-mammalian models for hair cell regeneration. Brain Res 1277:12–23.

Brunetti R, Gissi C, Pennati R, Caicci F, Gasparini F, Manni L. 2015. Morphological evidence that the molecularly determined *Ciona intestinalis* type A and type B are different species: *Ciona robusta* and *Ciona intestinalis*. J Zool Syst Evol Res 53:186–93.

Brunetti R, Manni L, Mastrototaro F, Gissi C, Gasparini F. 2017. Fixation, description and DNA barcode of a neotype for *Botryllus schlosseri* (Pallas, 1766) (Tunicata, Ascidiacea). Zootaxa 4353:29–50.

Burighel P, Caicci F, Manni L. 2011. Hair cells in non-vertebrate models: lower chordates and molluscs. Hear Res 273:14–24.

Burighel P, Caicci F, Zaniolo G, Gasparini F, Degasperi V, Manni L. 2008. Does hair cell differentiation predate the vertebrate appearance? Brain Res Bull 75:331–4.

Burighel P, Lane NJ, Gasparini F, Tiozzo S, Zaniolo G, Carnevali MDC, Manni L. 2003. Novel, secondary sensory cell organ in ascidians: in search of the ancestor of the vertebrate lateral line. J Comp Neurol 461:236–49.

Burns JC, Stone JS. 2017. Development and regeneration of vestibular hair cells in mammals. Semin Cell Dev Biol 65:96–105.

Caicci F, Degasperi V, Gasparini F, Zaniolo G, Del Favero M, Burighel P, Manni L. 2010. Variability of hair cells in the coronal organ of ascidians (Chordata, Tunicata). Can J Zool 88:567–78.

Caicci F, Gasparini F, Rigon F, Zaniolo G, Burighel P, Manni L. 2013. The oral sensory structures of Thaliacea (Tunicata) and consideration of the evolution of hair cells in Chordata. J Comp Neurol 521:2756–71.

Chagnaud BP, Engelmann J, Fritzsch B, Glover JC, Straka H. 2017. Sensing external and self-motion with hair cells: a comparison of the lateral line and vestibular systems from a developmental and evolutionary perspective. Brain Behav Evol 90:98–116.

Cima F, Ballarin L, Caicci F, Franchi N, Gasparini F, Rigon F, Schiavon F, Manni L. 2015. Life history and ecological genetics of the colonial ascidian *Botryllus schlosseri*. Zool Anz 257:54–70.

Cima F, Manni L, Basso G, Fortunato E, Accordi B, Schiavon F, Ballarin L. 2010. Hovering between death and life: natural apoptosis and phagocytes in the blastogenetic cycle of the colonial ascidian *Botryllus schlosseri*. Dev Comp Immunol 34:272–85.

Coffin AB, Reinhart KE, Owens KN, Raible DW, Rubel EW. 2009. Extracellular divalent cations modulate aminoglycoside-induced hair cell death in the zebrafish lateral line. Hear Res 253:42–51.

Dabdoub A, Fritzsch B, Popper AN, Fay RR, editors. 2016. The primary auditory neurons of the mammalian cochlea. Springer handbook of auditory research. New York: Springer.

Degasperi V, Gasparini F, Shimeld SM, Sinigaglia C, Burighel P, Manni L. 2009. Muscle differentiation in a colonial ascidian: organisation, gene expression and evolutionary considerations. BMC Dev Biol 9:48.

Ding L, Cheng R, Hu Y, Takahashi Y, Jenkins AJ, Keech AC, Humphries KM, Gu X, Elliott MH, Xia X, et al. 2014. Peroxisome proliferator-activated receptor α protects capillary pericytes in the retina. Am J Pathol 184:2709–20.

Elliott KL, Kersigo J, Pan N, Jahan I, Fritzsch B. 2017. Spiral ganglion neuron projection development to the hindbrain in mice lacking peripheral and/or central target differentiation. Front Neural Circuits 11:25.

Fan C, Zou S, Wang J, Zhang B, Song J. 2016. Neomycin damage and regeneration of hair cells in both mechanoreceptor and electroreceptor lateral line organs of the larval Siberian sturgeon (*Acipenser baerii*). J Comp Neurol 524:1443–56.

Franchi N, Ballin F, Manni L, Schiavon F, Basso G, Ballarin L. 2016. Recurrent phagocytosis-induced apoptosis in the cyclical generation change of the compound ascidian *Botryllus schlosseri*. Dev Comp Immunol 62:8–16.

Fritzsch B, Elliott KL. 2017. Gene, cell, and organ multiplication drives inner ear evolution. Dev Biol 431:3–15.

Gans C, Northcutt RG. 1983. Neural crest and the origin of vertebrates: a new head. Science 220:268–73.

Gasparini F, Burighel P, Manni L, Zaniolo G. 2008. Vascular regeneration and angiogenic-like sprouting mechanism in a compound ascidian is similar to vertebrates. Evol Dev 10:591–605.

Gasparini F, Caicci F, Rigon F, Zaniolo G, Burighel P, Manni L. 2013a. Cytodifferentiation of hair cells during the development of a basal chordate. Hear Res 304: 188–99.

Gasparini F, Caicci F, Rigon F, Zaniolo G, Manni L. 2014. Testing an unusual *in vivo* vessel network model: a method to study angiogenesis in the colonial tunicate *Botryllus schlosseri*. Sci Rep 4:6460.

Gasparini F, Degasperi V, Shimeld SM, Burighel P, Manni L. 2013b. Evolutionary conservation of the placodal transcriptional network during sexual and asexual development in chordates. Dev Dyn 242:752–66.

Gasparini F, Manni L, Cima F, Zaniolo G, Burighel P, Caicci F, Franchi N, Schiavon F, Rigon F, Campagna D, et al. 2015. Sexual and asexual reproduction in the colonial ascidian *Botryllus schlosseri*. Genesis 53:105–20.

Gasparini F, Shimeld SM, Ruffoni E, Burighel P, Manni L. 2011. Expression of a Musashi-like gene in sexual and asexual development of the colonial chordate *Botryllus schlosseri* and phylogenetic analysis of the protein group. J Exp Zool B Mol Dev Evol 316B:562–73.

Hou X, Shen YH, Li C, Wang F, Zhang C, Bu P, Zhang Y. 2010. PPARalpha agonist fenofibrate protects the kidney from hypertensive injury in spontaneously hypertensive rats via inhibition of oxidative stress and MAPK activity. Biochem Biophys Res Commun 394:653–9.

Huth ME, Ricci AJ, Cheng AG. 2011. Mechanisms of aminoglycoside ototoxicity and targets of hair cell protection. Int J Otolaryngol 2011:937861.

Kawamura K, Tachibana M, Sunanaga T. 2008. Cell proliferation dynamics of somatic and germline tissues during zooidal life span in the colonial tunicate *Botryllus primigenus*. Dev Dyn 237:1812–25.

Kocot KM, Tassia MG, Halanych KM, Swalla BJ. 2018. Phylogenomics offers resolution of major tunicate relationships. Mol Phylogenet Evol 121:166–73.

Mackie GO, Burighel P, Caicci F, Manni L. 2006. Innervation of ascidian siphons and their responses to stimulation. Can J Zool 84:1146–62.

Manni L, Burighel P. 2006. Common and divergent pathways in alternative developmental processes of ascidians. Bioessays 28:902–12.

Manni L, Gasparini F, Hotta K, Ishizuka KJ, Ricci L, Tiozzo S, Voskoboynik A, Dauga D. 2014. Ontology for the asexual development and anatomy of the colonial chordate *Botryllus schlosseri*. PLoS One 9:e96434.

Manni L, Lane NJ, Burighel P, Zaniolo G. 2001. Are neural crest and placodes exclusive to vertebrates?. Evol Dev 3:297–8.

Manni L, Zaniolo G, Cima F, Burighel P, Ballarin L. 2007. *Botryllus schlosseri*: a model ascidian for the study of asexual reproduction. Dev Dyn 236:335–52.

Northcutt RG, Gans C. 1983. The genesis of neural crest and epidermal placodes: a reinterpretation of vertebrate origins. Q Rev Biol 58:1–28.

Park C, Ji H-M, Kim S-J, Kil S-H, Lee JN, Kwak S, Choe S-K, Park R. 2017. Fenofibrate exerts protective effects against gentamicin-induced toxicity in cochlear hair cells by activating antioxidant enzymes. Int J Mol Med 39:960–8.

Patthey C, Schlosser G, Shimeld SM. 2014. The evolutionary history of vertebrate cranial placodes—I: cell type evolution. Dev Biol 389:82–97.

Pennati R, Ficetola GF, Brunetti R, Caicci F, Gasparini F, Griggio F, Sato A, Stach T, Kaul-Strehlow S, Gissi C, et al. 2015. Morphological differences between larvae of the *Ciona intestinalis* species complex: hints for a valid taxonomic definition of distinct species. PLoS One 10:e0122879.

Pohlert T. 2014. The pairwise multiple comparison of mean ranks package (PMCMR). R package, 27 (http://CRANR-project.org/package=PMCMR).

R Core Team. 2017. R: a language and environment for statistical computing. Vienna, Austria: R Foundation for statistical Computing (http://wwwR-project.org/).

Ricci L, Chaurasia A, Lapébie P, Dru P, Helm RR, Copley RR, Tiozzo S. 2016. Identification of differentially expressed genes from multipotent epithelia at the onset of an asexual development. Sci Rep 6:27357.

Rigon F, Gasparini F, Shimeld SM, Candiani S, Manni L. 2018. Developmental signature, synaptic connectivity and neurotransmission are conserved between vertebrate hair cells and tunicate coronal cells. J Comp Neurol 526:957–71.

Rigon F, Stach T, Caicci F, Gasparini F, Burighel P, Manni L. 2013. Evolutionary diversification of secondary mechanoreceptor cells in tunicata. BMC Evol Biol 13:112.

Schlosser G, Patthey C, Shimeld SM. 2014. The evolutionary history of vertebrate cranial placodes II. Evolution of ectodermal patterning. Dev Biol 389:98–119.

Sienknecht UJ, Köppl C, Fritzsch B. 2014. Evolution and development of hair cell polarity and efferent function in the inner ear. Brain Behav Evol 83:150–61.

Tiozzo S, Ballarin L, Burighel P, Zaniolo G. 2006. Programmed cell death in vegetative development: apoptosis during the colonial life cycle of the ascidian *Botryllus schlosseri*. Tissue Cell 38:193–201.

Whitfield TT. 2002. Zebrafish as a model for hearing and deafness. J Neurobiol 53:157–71.

Xu J, Ueno H, Xu CY, Chen B, Weissman IL, Xu P-X. 2017. Identification of mouse cochlear progenitors that develop hair and supporting cells in the organ of Corti. Nat Commun 8:15046.

Yousefipour Z, Oyekan A, Newaz M. 2010. Interaction of oxidative stress, nitric oxide and peroxisome proliferator activated receptor gamma in acute renal failure. Pharmacol Ther 125:436–45.

Zaniolo G, Lane NJ, Burighel P, Manni L. 2002. Development of the motor nervous system in ascidians. J Comp Neurol 443:124–35.